Mesoporous Microspheres

DOI: 10.1002/ange.201307608

A General "Surface-Locking" Approach toward Fast Assembly and Processing of Large-Sized, Ordered, Mesoporous Carbon Microspheres**

Zhangxiong Wu, Winston Duo Wu, Wenjie Liu, Cordelia Selomulya, Xiao Dong Chen, and Dongyuan Zhao**

Ordered mesoporous carbons (OMCs) are potentially useful in, for example, adsorption and separation, energy storage and conversion, and catalysis.[1] There are many methods to adjust structure and porosity, and to introduce functionality.[2] Comparatively, control of morphology, size, and uniformity in OMCs is much more difficult, although many disordered porous carbon nanospheres with uniform sizes have been reported.[3] More challengingly, little success has been achieved in realizing particle engineering in OMCs at the micrometer length scale for assembling large-sized microspheres and to deploy processing technology for scalable particle fabrication, both of which may be essential to bring many potential applications of OMCs into reality.

Most reported OMCs are of small size, irregular shape, and/or poor size uniformity. Bottlenecks may be encountered when they are applied to dynamic adsorption, chromatography, and catalysis. To this end, uniform microspheres with large sizes are desirable. In addition, fast and scalable production of OMCs is still open for improvement.[4] Aerosol methods that can couple colloid chemistry and fast drying process are low-cost and productive to generate porous particles.[5] Porous (occasionally ordered) carbon microspheres have been fabricated by aerosol methods, such as ultrasonic spray pyrolysis and aerosol-assisted self-assembly.[6] However, these routes generally produce particles with small sizes (sub- to a few micrometers), poor size uniformity, only low to medium surface areas, small pore volumes, nonuniform pore sizes, and poor pore connectivity and openness (especially at the surface). Fabrication of uniform and large-sized OMC microspheres is still very challenging. For aerosol methods, generation of uniform and large droplets is difficult; a droplet with a large size tends to deform upon fast drying; and a droplet boundary requires strict control to avoid particle coalescence. For other solution-growth methods, growth of uniform polymer microspheres is difficult, and a long time is required.[7] In both classes of methods, an extra mesostructuring process can add to the complexity and difficulty to control particle size and morphology.

Herein, we demonstrate a general "surface-locking" approach, in which the evaporation-induced self-assembly (EISA) strategy and a unique microfluidic jet spray drying technology[8] are coupled for the first time, for fast assembly and continuous processing of mesoporous microspheres. In this approach, the colloidal chemistry of a droplet suspension is rapidly driven far from equilibrium so that the surface of the drying droplet can be efficiently "locked" through the formation of a rigid crust. It thus enables instant formation of discrete microspheres from molecular precursors and localization of structure assembly and colloid chemistry inside the "locked" droplet. The "surface-locking" mechanism that governs dynamic evolution of morphology, composition, and mesostructure under fast drying conditions is delineated. With this novel approach, an unprecedented type of OMC microsphere is obtained.

The process involves a jet of an acidic ethanolic solution containing a template (Pluronic F127), a carbon precursor (resol), and a pre-hydrolyzed tetraethylorthosilicate (TEOS) being broken up to large and uniform droplets, which are then rapidly (within 2 s) dried into hybrid microspheres (see experimental details in Supporting Information Section S1 and Figure S1–4). The key to obtaining microspheres within only 2 s lies in the formation of silica-rich crusts which act against particle coalescence and the presence of strong electrostatic forces which act against particle deformation. The hybrid microspheres are then converted into OMC microspheres with large size, excellent uniformity, ordered mesopores, high surface area, open and large porosity, and hollow architecture.

Hybrid (F127/phenolic resin/silica) microspheres can be obtained at a drying temperature of 160 °C with a production rate of approximately 30 g (equivalently, ca. 5 g of OMC microspheres) per hour per nozzle (Figure S5). They are uniform (ca. 80 μm in size) and smooth (Figure S6). The resulting OMC microspheres preserve the uniform spherical morphology with a size of approximately 61.0 μm (Figure 1 a)

[*] Dr. Z. X. Wu, Dr. W. J. Liu, Prof. Dr. C. Selomulya, Prof. Dr. D. Y. Zhao
Department of Chemical Engineering, Monash University
Wellington Road, Clayton, VIC 3800 (Australia)
E-mail: cordelia.selomulya@monash.edu
Dr. W. D. Wu, Prof. Dr. X. D. Chen
College of Chemistry, Chemical Engineering and Materials Science
Soochow University, Suzhou, Jiangsu 215123 (P. R. China)
Prof. Dr. D. Y. Zhao
Department of Chemistry and Laboratory of Advanced Materials
Fudan University
Shanghai 200433 (P. R. China)
E-mail: dyzhao@fudan.edu.cn
Homepage: http://www.mesogroup.fudan.edu.cn/

[**] Financial support from the Australian Research Council (DP120101194) is much appreciated. We acknowledge use of the facilities within the Monash Centre for Electron Microscopy.

Supporting information (experimental details) for this article is available on the WWW under http://dx.doi.org/10.1002/anie.201307608.

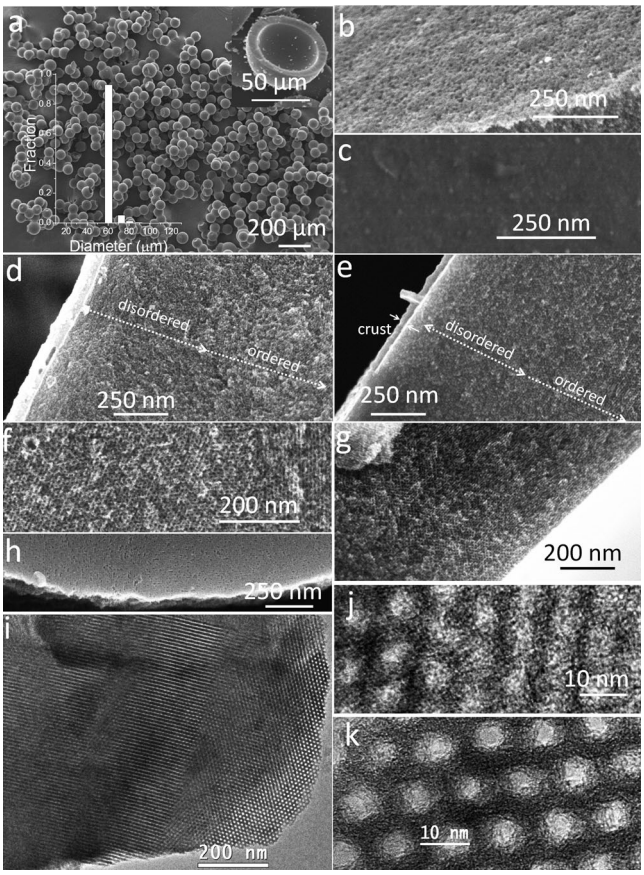

Figure 1. SEM (a), HRSEM (b–h), and TEM (i–k) images of the OMC microspheres (a, b, d, and f–j) and the intermediate silica/carbon composite microspheres (c, e, and k) at the external surfaces (b, c), external layers (d, e), middle part (f), inner layer (g), and internal surface (h); Insets in (a) are the particle size distribution and half of a magnified hollow sphere. The OMC microspheres were obtained at 160 °C, followed by carbonization at 900 °C and silica removal.

as a result of thermal shrinkage (56 %). Interestingly, they are hollow with a shell thickness of approximately 9 μm and a cavity diameter of about 43 μm (inset in Figure 1 a and Figure S7). Such hollow microstructures have attracted attention.[9] They possess a highly ordered hexagonal mesostructure (space group *p6mm*; Figure S8), indicating that the structure assembly proceeds quite well, although the temperature is as high as 160 °C and the evaporation time is only about 2 s. This is a significant advance over the conventional EISA synthesis of OMCs that takes 5–8 h for solvent evaporation and a day for thermosetting.[2b,10] While the overall mesostructure ordering is high, there are ordering gradients in the OMC microspheres. They show open and uniform but disordered mesopores at the external surfaces (Figure 1 b, and Figure S9a–d). Across a carbon shell, there is a thin (ca. 500 nm) external layer with disordered mesopores (Figure 1 d and Figures S10a, j). Inwards, highly ordered mesopores are present throughout (Figure 1 f–h and Figure S10b–j). A microtomed carbon slice also shows a thin disordered layer and then a thick ordered shell (Figure S11 and 1i, j). Such a sharp ordering gradient is related to the temperature and mass gradients created during fast drying.

To extract key parameters for evolution of the microspheres, two control experiments were conducted (Section S1.2). Without resols, dramatic droplet deformation occurred during the fast drying, leading to crumpled silica microparticles (Figure S12). The stability of a liquid droplet depends on the interplay between capillary and electrostatic forces.[11] Without resols, as drying proceeds, the electrostatic forces gradually weaken and the surfaces become increasingly elastic as a result of the fast growth of the silica. Therefore, the capillary forces that drive droplet deformation can overcome the electrostatic forces that stabilize sphericity, leading to crumpling. In contrast, resols can strengthen the electrostatic forces through hydrogen bonding, and the viscous nature of resols helps to relieve elastic stress against deformation. Even a lower amount of resols in a F127/TEOS system can avoid droplet deformation (Figure S13). Without TEOS, droplet deformation can be avoided, but microspheres cannot be obtained. The reason lies in the low glass-transition temperature (T_g). The template F127 has $T_g \approx -64$ °C, while the T_g of resols is even lower. Thermosetting of resols is very limited in 2 s. Even a drying temperature of 200 °C still generates sticky gels without silica (Figure S14). Only with resols cross-linked to solid phenolic species, can non-sticky polymer microspheres be obtained, which is extremely difficult to achieve within 2 s. Thus, it is assumed that thin and rigid silica-rich crusts are formed during fast drying, which can "lock" the surfaces to obtain microspheres.

To verify the above assumption, the intermediate silica/carbon composite microspheres were fully characterized and compared with the film control sample (Section S1.5).[10] The composite microspheres have identical particle size (Figure S15) and structure parameters (Figure S8) to those (Figure 1 a, and Figure S8) of the final OMC microspheres. Therefore, no phase separation occurs during fast drying. Their external surfaces are dense (Figure 1 c and Figure S16a). With a thin outer layer peeled off, non-porous, disordered, and ordered porous areas are observed from outside to inside (Figure S16b,c). Along a typical shell, there is a dense crust approximately 25 nm thick (Figure 1 e) and a subsequent disordered layer of about 500 nm (Figure 1 e and S17). Inwards, ordered mesopores are present throughout (Figure S17). TEM images also show the presence of dense, disordered, and highly ordered areas (Figure S18, and 1k). In contrast, no ordering gradient is present in the control sample (Figure S19). The composite microspheres have an overall silica content of around 56 wt %, while their surfaces are silica-dominant (> 90 wt %) (Figure S20). In addition, they show very low N_2 adsorption (Figure 2 b) with a surface area of only about 11 $m^2 g^{-1}$, far smaller than that (358 $m^2 g^{-1}$) of the control sample (Figure 2 a).[10] Moreover, their "true" density (ca. 1.16 $g cm^{-3}$) is much lower than that (ca. 2.1 $g cm^{-3}$) of the control sample (Figure S21a,b). After crushing, their surface area increases to 327 $m^2 g^{-1}$ (Figure 2 c), close to that of the control sample. The above results clearly verify the existence of dense silica-rich crusts.

Based on the above results, an insight "surface-locking" mechanism (Scheme 1) that governs the dynamic evolution of morphology, composition, and mesostructure under fast drying conditions is proposed. The initial droplet (Sche-

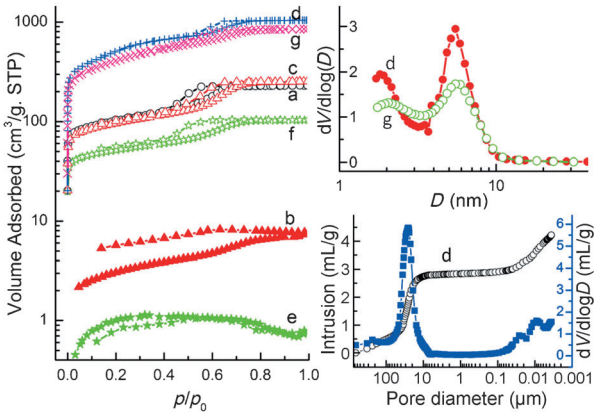

Figure 2. N_2 sorption and mercury intrusion (bottom right) results of the mesoporous film control sample (a), the carbonized silica/carbon composite microspheres obtained at a drying temperature of 160 (b, c) and 170 °C (e, f) before (b, e) and after (c, f) crushing, and the final OMC microspheres obtained at 160 (d) and 170 °C (g).

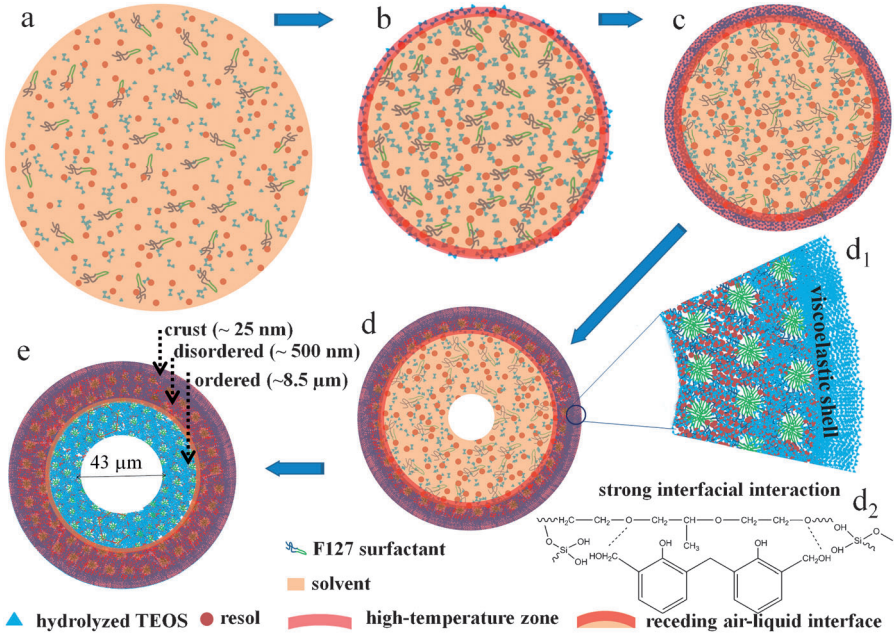

Scheme 1. The dynamic "surface-locking" mechanism during fast drying: a) the initial droplet, b) temperature ramp and silica growth at the surface, c) formation of silica-rich crust that "locks" the droplet, d) emergence of disordered mesostructure at the interface and hollow cavity inside, d_1) magnified area at the external surface showing the silica-rich crust and the three-component composite micelle assemblies, d_2) a simple model showing the strong interfacial electrostatic interactions, and e) shift of the air–liquid interface and growth of both disordered and ordered mesostructures, and hollow cavity.

me 1 a) has a radius of about 90 μm (Figure S3), far smaller than its capillary length (> 1.42 mm, Section S2), suggesting that gravity has no distorting effect on sphericity. Initially, the droplet is homogeneous. Its drying process can be divided into three stages.[12] The first one is a warm-up period, which is extremely short. The second one is the constant drying-rate period when evaporation proceeds constantly with the droplet surface saturated with free solvent (ethanol) and the droplet temperature maintained at the wet-bulb temperature (ca. 35 °C).[13] This stage is also very short owing to the limited amount of free ethanol.[14] The final stage is the dominant falling-drying-rate period when the droplet surface temperature quickly increases to close to 160 °C and the droplet shrinks rapidly as solvent evaporates. Meanwhile, rapid growth of silica at the droplet's surface occurs (Scheme 1 b) as a result of three nonlinear effects. Firstly, because of the lower amount of liquid at the surface than in the bulk of the droplet and the retarded heat transfer, the surface temperature is much higher than that of the interior, promoting silica growth at the surface. Secondly, the acid catalyst (HCl) diffuses outwards with evaporation so that TEOS at the interface is subject to a more hydrolytic environment. Thirdly, when silica particles are formed at the interface, the time that they need to take to diffuse across the radius of the droplet to homogenize it is more than 10^4 s (Section S3), far longer than the time for the solvent to evaporate (< 2 s). Such a huge time difference means that the drying kinetics drive the suspension far from equilibrium so that the surface is enriched with silica while the interior remains at its initial molar ratios (Scheme 1 b). As the solvent continues to evaporate and temperature increases, silica particles quickly pile up, leading to the formation of a surface crust well before complete solvent evaporation inside the droplet (Scheme 1 c). As a result, the droplet is "locked" without further inward shrinkage and its size is "frozen" by the rigidity of the crust. Thereafter, the precursors diffuse outward (outward shrinkage) with further solvent evaporation, leading to the emergence and growth of a hollow cavity (Scheme 1 d). Inside the crust, tiny menisci are formed among the silica particles, creating small tensions that simultaneously pull liquid outward and drive particles inward, thus keeping the particles wetted with solvent and some resols before complete drying. Thus, the crust presents viscoelastic behavior. As drying goes, the crust becomes increasingly elastic and the droplet tends to buckle. Fortunately, the strong electrostatic forces (especially resol-induced hydrogen bonding) can stabilize the crust against deformation, and the elastic stress can be relieved through viscous flow of resols so that sphericity is maintained (Scheme 1 d). Without resols, capillary deformation overcomes electrostatic forces, triggering particle crumpling (Figure S12). Without silica, the surface cannot be "locked" to obtain microspheres (Figure S14).

The mesostructuring during the fast drying is path-dependent. Formation of the unstructured crust (Scheme 1 c–e) is due to the fast growth of silica at the surface where the temperature is highest and the template F127 is far

below its critical micelle concentration (CMC) as a result of its higher diffusibility and solubility compared to silica particles. Under this crust, a mesostructure gradient arises because of the radical temperature and composition gradients. At the falling-drying-rate period, the droplet surface temperature rises to 160 °C, while the temperature at the air–liquid interface approaches the boiling point of ethanol (ca. 78 °C), and the temperature in the interior liquid is well below 78 °C. Mesostructuring takes place first at the interface (Scheme 1 d) because CMC is achieved here first and the presence of the air–liquid interface may serve as a nucleating surface.[5a,b] Then, mesostructure grows radially inward as CMC is continuously achieved. Because mesostructuring at the interface occurs near the boiling point of ethanol, it is extremely fast and the subsequent temperature increase to 160 °C may also modify the mesophase, leading to a disordered mesostructure. As drying continues, the air–liquid interface frontier shifts inward until there is no more liquid available, leading to the formation of a disordered layer (Scheme 1 d,e). As ethanol diffuses and evaporates so fast, the shift path of the instable air–liquid interface is limited to approximately 500 nm. Structuration under the interface proceeds well forming ordered domains (Scheme 1 e).

To further validate the "surface-locking" mechanism, a higher drying temperature of 170 °C was adopted. The resulting carbon microspheres are highly monodisperse (Figure 3 a,b), with a larger size (ca. 68 μm) than that of those obtained at 160 °C (ca. 61 μm). The reason for the improvements in sphericity, monodispersity, and size increase, is that the higher drying temperature leads to faster formation of denser and thicker silica crusts. Thus, the droplet surfaces can be "locked" and the sizes can be "frozen" more rapidly and efficiently. The composite microspheres obtained at 170 °C show a negligible N_2 porosity which approaches to that of the control sample after crushing the microspheres (Figure 2 e,f) and a very low "true" density of approximately 0.9 g cm^{-3} (Figure S21d). Their non-porous crusts are about 30 nm thick (Figure S22b), a little thicker than that of those obtained at 160 °C (ca. 25 nm). The disordered layer (Figure S22c–e) is much thicker (ca. 4.7 μm vs. ca. 500 nm). This change is because the higher temperature leads to a longer shift path of the instable air–liquid interface in the drying droplets. Even at 170 °C, the structure assembly still proceeds well in the inner part with ordered mesopores observed (ca. 2.8 μm in thickness; Figure S22f–h). After silica removal, the carbon microspheres show open mesopores at the surfaces (Figure 3 c), followed by a disordered and ordered layer of about 4.7 and 2.8 μm (Figure 3 d,e).

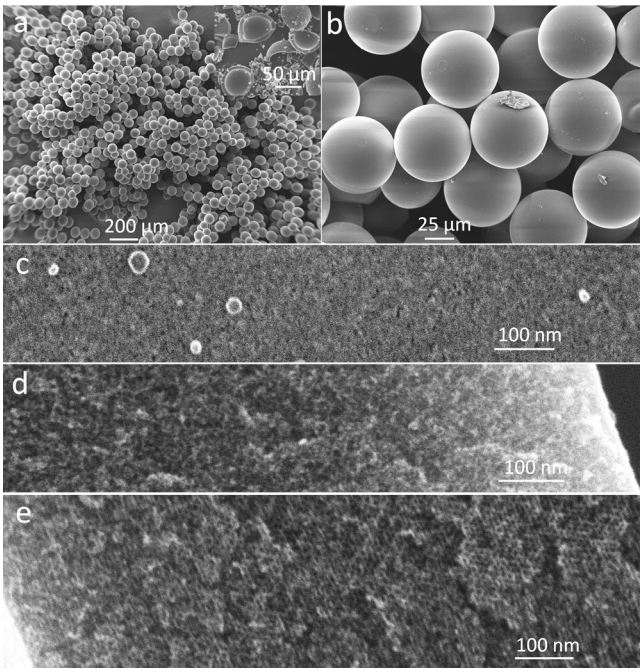

Figure 3. SEM (a, b, and inset in a) and HRSEM (c–e) images at the external surface (c) and the cross-section (d, e) of the final carbon microspheres obtained at a drying temperature of 170 °C.

The "surface-locking" approach can be adopted to synthesize other mesoporous microspheres that are hard to obtain by other methods. For example, mesoporous silica microspheres (Figure S23a,b) can be formed. In addition, metal oxides (such as alumina), can play a similar "surface-locking" role as silica. Thus, mesoporous metal oxide (such as alumina, Figure S23c–f) microspheres can be obtained.

The OMC microspheres obtained at 160 °C show type IV N_2 sorption isotherms, with a surface area and pore volume of approximately 1930 m^2 g^{-1} and 1.62 cm^3 g^{-1}, and bimodal mesopores at about 2.0 and 5.5 nm (Figure 2 d), while those obtained at 170 °C show relatively smaller surface area and pore volume (ca. 1530 m^2 g^{-1} and 1.32 cm^3 g^{-1}), and wider pore size distribution (Figure 2 g). The gently crushed OMC microspheres (Figure S24) show narrow macropores at about 42 μm (Figure 2 d, bottom right, blue trace), correlating with the hollow cavity size. The porosity of the OMC microspheres is up to 90 %, with a bulk and "true" density of 0.191 and 2.15 g cm^{-3}, respectively (Figure S21c).

The integration of a range of desirable properties and the capability of scalable synthesis makes the OMC microspheres potentially very useful. As a proof-of-concept, they can be efficiently packed for efficient dynamic separation. For example, highly concentrated dye molecules can be rapidly removed from pure water (Figure S25).

In summary, we have demonstrated a novel "surface-locking" approach, in which the EISA strategy is integrated into the novel microfluidic jet spray drying technology, for fast assembly and scalable processing of OMC microspheres with a range of desirable properties, which make them highly attractive for a variety of applications. The importance of the two key factors for evolution of microspheres, namely, the formation of surface silica-rich crusts, and presence of strong electrostatic forces, has been illustrated. The innovative "surface-locking" mechanism that governs the dynamic morphology and composition evolution, and the path-dependent mesostructuring under extremely fast drying conditions has been delineated. Metal oxides may also play a similar "surface-locking" role to silica. This would pave the way for the assembly and processing of a variety of novel mesoporous microspheres with tailored properties and functionality.

Received: August 29, 2013
Published online: November 12, 2013

Keywords: carbon microspheres · interfacial assembly · mesoporous materials · microfluidics · spray drying

[1] a) M. E. Davis, *Nature* **2002**, *417*, 813; b) C. Liang, Z. Li, S. Dai, *Angew. Chem.* **2008**, *120*, 3754; *Angew. Chem. Int. Ed.* **2008**, *47*, 3696; c) A. Stein, Z. Y. Wang, M. A. Fierke, *Adv. Mater.* **2009**, *21*, 265; d) Z. X. Wu, D. Y. Zhao, *Chem. Commun.* **2011**, *47*, 3332; e) Y. Zhai, Y. Dou, D. Zhao, P. F. Fulvio, R. T. Mayes, S. Dai, *Adv. Mater.* **2011**, *23*, 4828.

[2] a) S. H. Joo, S. J. Choi, I. Oh, J. Kwak, Z. Liu, O. Terasaki, R. Ryoo, *Nature* **2001**, *412*, 169; b) Y. Meng, D. Gu, F. Q. Zhang, Y. F. Shi, H. F. Yang, Z. Li, C. Z. Yu, B. Tu, D. Y. Zhao, *Angew. Chem.* **2005**, *117*, 7215; *Angew. Chem. Int. Ed.* **2005**, *44*, 7053; c) C. D. Liang, S. Dai, *J. Am. Chem. Soc.* **2006**, *128*, 5316; d) Z. Wu, W. Li, P. A. Webley, D. Zhao, *Adv. Mater.* **2012**, *24*, 485; e) A. H. Lu, J. J. Nitz, M. Comotti, C. Weidenthaler, K. Schlichte, C. W. Lehmann, O. Terasaki, F. Schüth, *J. Am. Chem. Soc.* **2010**, *132*, 14152.

[3] a) Y. Fang, D. Gu, Y. Zou, Z. X. Wu, F. Y. Li, R. C. Che, Y. H. Deng, B. Tu, D. Y. Zhao, *Angew. Chem.* **2010**, *122*, 8159; *Angew. Chem. Int. Ed.* **2010**, *49*, 7987; b) M. M. Titirici, M. Antonietti, *Chem. Soc. Rev.* **2010**, *39*, 103; c) J. Liu, S. Z. Qiao, H. Liu, J. Chen, A. Orpe, D. Zhao, G. Q. Lu, *Angew. Chem.* **2011**, *123*, 6069; *Angew. Chem. Int. Ed.* **2011**, *50*, 5947; d) A. H. Lu, T. Sun, W. C. Li, Q. Sun, F. Han, D. H. Liu, Y. Guo, *Angew. Chem.* **2011**, *123*, 11969; *Angew. Chem. Int. Ed.* **2011**, *50*, 11765; e) H. Xu, J. Guo, K. S. Suslick, *Adv. Mater.* **2012**, *24*, 6028; f) R. Liu, S. M. Mahurin, C. Li, R. R. Unocic, J. C. Idrobo, H. Gao, S. J. Pennycook, S. Dai, *Angew. Chem.* **2011**, *123*, 6931; *Angew. Chem. Int. Ed.* **2011**, *50*, 6799.

[4] a) C. Xue, B. Tu, D. Zhao, *Adv. Funct. Mater.* **2008**, *18*, 3914; b) J. Wang, C. Xue, Y. Lv, F. Zhang, B. Tu, D. Zhao, *Carbon* **2011**, *49*, 4580.

[5] a) Y. Lu, R. Ganguli, C. A. Drewien, M. T. Anderson, C. J. Brinker, W. Gong, Y. Guo, H. Soyez, B. Dunn, M. H. Huang, J. I. Zink, *Nature* **1997**, *389*, 364; b) Y. Lu, H. Fan, A. Stump, T. L. Ward, T. Rieker, C. J. Brinker, *Nature* **1999**, *398*, 223; c) Q. Hu, R. Kou, J. Pang, T. L. Ward, M. Cai, Z. Yang, Y. Lu, J. Tang, *Chem. Commun.* **2007**, 601; d) C. Boissiere, D. Grosso, A. Chaumonnot, L. Nicole, C. Sanchez, *Adv. Mater.* **2011**, *23*, 599; e) C. K. Tsung, J. Fan, N. Zheng, Q. Shi, A. J. Forman, J. Wang, G. D. Stucky, *Angew. Chem.* **2008**, *120*, 8810; *Angew. Chem. Int. Ed.* **2008**, *47*, 8682; f) I. V. Melnyk, Y. L. Zub, E. Veron, D. Massiot, T. Cacciaguerra, B. Alonso, *J. Mater. Chem.* **2008**, *18*, 1368.

[6] a) Y. Yan, F. Q. Zhang, Y. Meng, B. Tu, D. Y. Zhao, *Chem. Commun.* **2007**, 2867; b) W. H. Suh, J. K. Kang, Y. H. Suh, M. Tirrell, K. S. Suslick, G. D. Stucky, *Adv. Mater.* **2011**, *23*, 2332; c) See Ref. [3e]; d) J. D. Atkinson, M. E. Fortunato, S. A. Dastgheib, M. Rostam-Abadi, M. J. Rood, K. S. Suslick, *Carbon* **2011**, *49*, 587; e) M. E. Fortunato, M. Rostam-Abadi, K. S. Suslick, *Chem. Mater.* **2010**, *22*, 1610.

[7] a) Y. Pan, M. Ju, C. Wang, L. Zhang, N. Xu, *Chem. Commun.* **2010**, *46*, 3732; b) L. Guo, J. Zhang, Q. He, L. Zhang, J. Zhao, Z. Zhu, W. Wu, J. Shi, *Chem. Commun.* **2010**, *46*, 7127; c) D. Long, F. Lu, R. Zhang, W. Qiao, L. Zhan, X. Liang, L. Ling, *Chem. Commun.* **2008**, 2647.

[8] a) W. D. Wu, S. X. Lin, X. D. Chen, *AIChE J.* **2011**, *57*, 1386; b) W. D. Wu, R. Amelia, N. Hao, C. Selomulya, D. Zhao, Y. L. Chiu, X. D. Chen, *AIChE J.* **2011**, *57*, 2726.

[9] X. W. Lou, L. A. Archer, Z. Yang, *Adv. Mater.* **2008**, *20*, 3987.

[10] R. Liu, Y. Shi, Y. Wan, Y. Meng, F. Zhang, D. Gu, Z. Chen, B. Tu, D. Zhao, *J. Am. Chem. Soc.* **2006**, *128*, 11652.

[11] N. Tsapis, E. R. Dufresne, S. S. Sinha, C. S. Riera, J. W. Hutchinson, L. Mahadevan, D. A. Weitz, *Phys. Rev. Lett.* **2005**, *94*, 018302.

[12] K. Masters, *Spray Drying Handbook*, 5th ed. Longman Scientific and Technical, Singapore, **1991**.

[13] R. D. Ingebo, Vaporization rates and heat transfer coefficients for pure liquid drops, NACA Reports, TN 2368 **1951**.

[14] X. D. Chen, S. X. Q. Lin, *AIChE J.* **2005**, *51*, 1790.

